AJNR

Loss of Interhemispheric Connectivity in Patients with Lacunar Infarction Reflected by Diffusion-Weighted MR Imaging and Single-Photon Emission CT

Makiko Ishihara, Shin-ichiro Kumita, Hiromitsu Hayashi and Tatsuo Kumazaki

Loss of Interhemispheric Connectivity in Patients with Lacunar Infarction Reflected by Diffusion-Weighted MR Imaging and Single-Photon Emission CT

Makiko Ishihara, Shin-ichiro Kumita, Hiromitsu Hayashi, and Tatsuo Kumazaki

BACKGROUND AND PURPOSE: **Although decreased neuronal connectivity in white matter has been reported to be a key mechanism of vascular dementia, assessment of white matter changes by diffusion-weighted MR imaging in relation to measures of associative function has not been previously addressed. We evaluated the loss of interhemispheric neuronal connectivity in vascular dementia by measuring diffusional anisotropy of the corpus callosum and determining its relationship to the regional cortical activity as reflected by cortical perfusion.**

METHODS: **Nine patients with multiple lacunar infarction and six healthy volunteers (25–35 years old) were examined. We developed a method to determine the active cortical volume (ACV) by masking iodine-123 iodoamphetamine SPECT scans to eliminate the effect of brain atrophy. The anisotropic rate (AR) was calculated as a ratio of two perpendicular diffusion coefficients in diffusion-weighted MR imaging.**

RESULTS: **Compared with the ACVs of the healthy volunteers, there were significant decreases in the ACVs in the frontal associative areas in the patients, and these were significantly correlated with cognitive scores. The frontal ACVs showed good correlations with the AR of the anterior corpus callosum among all participants; however, only insignificant trends toward correlation were observed between these two parameters within the patient group.**

CONCLUSION: **A possible relationship between diffusional anisotropy of the anterior corpus callosum and frontal associative function was suggested; however, an estimation of the decrease in neuronal connectivity in patients with multiple lacunar infarction in terms of the deterioration in diffusional anisotropy requires further documentation.**

Data from functional neuroimaging (1, 2) and postmortem neuropathologic (3, 4) studies have shown that decreased neuronal connectivity in white matter may be a key mechanism of vascular dementia. The former studies have suggested a contribution of the diaschisis phenomenon between cortical and subcortical structures, and the latter studies have revealed actual histopathologic changes in subcortical structures. In particular, electron microscopic studies of Binswanger disease have revealed that the decreased number of nerve fibers in the anterior corpus callosum seems to play a contributory role in the development of dementia (4). However, direct assessment of white matter changes in vivo in relation to measures of cognitive impairment have not been previously addressed.

Because of the advance of ultrafast MR imaging, diffusion-weighted MR imaging, which permits in vivo measurement of random motion of tissue water molecules (5, 6), has matured into an easy-to-perform technique (7). The magnitude of diffusion, given by an apparent diffusion coefficient (ADC), varies with the direction of measurement because of water restriction by the myelin sheath (diffusional anisotropy), and this provides much information on the microstructural orientation of white matter (7–10), especially of major tracts, such as the corpus callosum (7, 8, 10). Recently, we reported the decreases of diffusional anisotropy of the anterior corpus callosum in association with multiple lacunar infarction and its possible relation to cognitive impairment (11). Because these findings are in agreement with the results of the electron microscopic studies of Binswanger disease (4), the histopathologic features of which are basically identical to those of multiple lacunar infarction (12), we hypothesized that our findings (11) reflect the number of damaged fibers and thus indicate the extent of decreased interhemispheric neuronal connectivity. Questions then arose as to the relation-

ship between the diffusional anisotropy of corpus callosum and actual associative function.

In quantitative measurements of cortical perfusion by radiotracer uptake, partial volume averaging of gray matter, white matter, and CSF spaces can induce significant inaccuracy (13), especially in the atrophic brain (14). To address this, we developed a method of assessing cortical perfusion in terms of active cortical volume (ACV). The ACV technique masks single-photon emission CT (SPECT) scans, instead of measuring the degree of perfusion reduction, to estimate actual cortical activity. The goals of the current study were, therefore, to determine whether ACV is feasible as an index of cortical activity in associative areas and to assess the relationship between ACV in associative areas and diffusional anisotropy of the corpus callosum. We discuss the possibility of estimating loss of neuronal connectivity in cases of multiple lacunar infarction in terms of the deterioration in diffusional anisotropy of the anterior corpus callosum, thereby providing new background information regarding vascular dementia.

Methods

Participants

We studied nine patients with multiple lacunar infarction (six men and three women; average age, 74 ± 8 years; range, 62–86 years) and poor cognitive levels as evaluated by minimental state examination (MMSE) (mean score, 17 ± 5; range, 10–23), and six healthy young adult volunteers (six men; average age, 30 ± 4 years; range, 25–35). Informed consent was obtained from every participant. Using a database of patients with multiple lacunar infarction in our laboratory, the study group was selected from persons who underwent brain SPECT and MR imaging within a 3-week interval. Every subject had a clinical history of repeat transient ischemic attack and hypertension and had multiple lacunae in the deep cerebral region around the perforating vessels revealed by routine T1- and T2-weighted MR imaging. We did not include patients with cortical lesions in order to eliminate the effect of direct cortical tissue damage.

Imaging Protocol

MR imaging data were acquired using a 1.5-T system (SignaHorizon, General Electric Yokokawa Medical Systems, Tokyo, Japan) at the maximum gradient strength of 23 mT/m and slew rate of 77 T/m per second with a quadrature head coil. A subject's head was carefully placed to ensure that the anterior-posterior commissure line was parallel to the axial gradient planes and axial sections. Routine MR imaging evaluation of 15 contiguous axial sections of the whole brain was performed using conventional spin-echo T1-weighted 420/10 (TR/TE) and fast spin echo T2-weighted 3500/100 (TR/TE$_{eff}$) images, with an echo train of 10, a field of view of 24 × 24 cm, an imaging matrix of 256 × 256, and a 6.5-mm section thickness with a 2.0-mm gap. For diffusion-weighted MR imaging, single-shot echo-planar imaging was used to obtain 12 to 14 contiguous axial 6500/120 sections, with a field of view of 24 × 24 cm, an imaging matrix of 128 × 128, and a 7.0-mm section with a 1.0-mm gap. The diffusion gradient pulses were applied with settings of b = 0 and b = 710 along the readout gradient axis (right to left, x-axis) and the phase gradient axis (anterior to posterior, y-axis), respectively; their duration was 25 milliseconds with a 29.2-millisecond gap.

SPECT data were acquired using a three-headed gamma camera Prism 3000 (Picker-Shimadzu International Inc, Kyoto, Japan), with low-energy high-resolution collimation and 5° projections over each 120° with 60 seconds of data collimation per projection, at 10 minutes after intravenous injection of 222 MBq of iodine-123 iodoamphetamine (^{123}I-IMP). After prefiltering the projection data with the standard 2D Butterworth filter, axial images parallel to the anterior-posterior commissure line were reconstructed with a 6.8-mm section thickness and a 1.0-mm gap. The reconstruction matrix of the SPECT scans was 128 × 128, and spatial resolution was 9 mm full width at half-maximum in the axial plane.

Determination of Diffusional Anisotropy

Three series of diffusion-weighted MR imaging data with a setting of b = 0 and b = 710 for each x- and y-axial direction were processed on an online computer system (Sun Sparc20) to create parametric ADC maps of each direction by using interactive data language software. For the calculation of ADC, the monoexponential intravoxel incoherent motion model (6) was used.

$$S(b_i = 710) = S(b = 0) * \exp(-b * ADC_i;) \; i = x, y$$

Therefore, the ADC value of each direction can be determined in each pixel from the relative signal intensities by solving the following equations:

$$ADC_x = \ln [S(b = 0)/S(b_x = 710)]/(710 - 0)$$

$$ADC_y = \ln [S(b = 0)/S(b_y = 710)]/(710 - 0)$$

where S is the signal intensity, b is the factor determined by the gradient strength, and each ADC_x and ADC_y is the ADC value in each axial direction. Region of interest (ROI) data of the ADC_x and ADC_y maps were extracted from the anterior and posterior parts of the corpus callosum and optic radiation (Fig 1). The ratio of ADC_x to ADC_y, namely, the anisotropic rate (AR) (AR = ADC_x/ADC_y × 100), was calculated as an index of diffusional anisotropy as in previous studies (15, 16). This index can be used to determine the main fiber orientation in a particular ROI. If the AR is greater than 1, the fibers are oriented in an x-axial direction; and if the AR is less than 1, the fibers are oriented in a y-axial direction.

Determination of ACV and Evaluation of the Relation to Neuronal Connectivity

For intersubject analysis, SPECT scans usually require normalization to counts in a certain reference area. In this study, the value of maximal counts measured in the visual cortex was used for normalization because there were no participants with reduced visual function in this study. Initially, brain uptake of greater than 80% of the maximal counts in the visual cortex was assumed to represent active cortical tissue and we defined it as the upper masking level. A lower masking level for eliminating pixels of white matter and CSF space from SPECT scans was also determined. After excluding scatter counts outside the brain, binary maps at the preliminary lower masking levels of 60%, 65%, and 70% of the maximal counts in the visual cortex of the subjects were created to determine which level results in a proportion of masked pixels closest to that of major white matter and CSF space, as has previously been calculated using manual thresholding of anatomic MR imaging (17). The ACV was thus defined as the regional ratio of the number of pixels above the 80% map to the number above the lower masking map as follows:
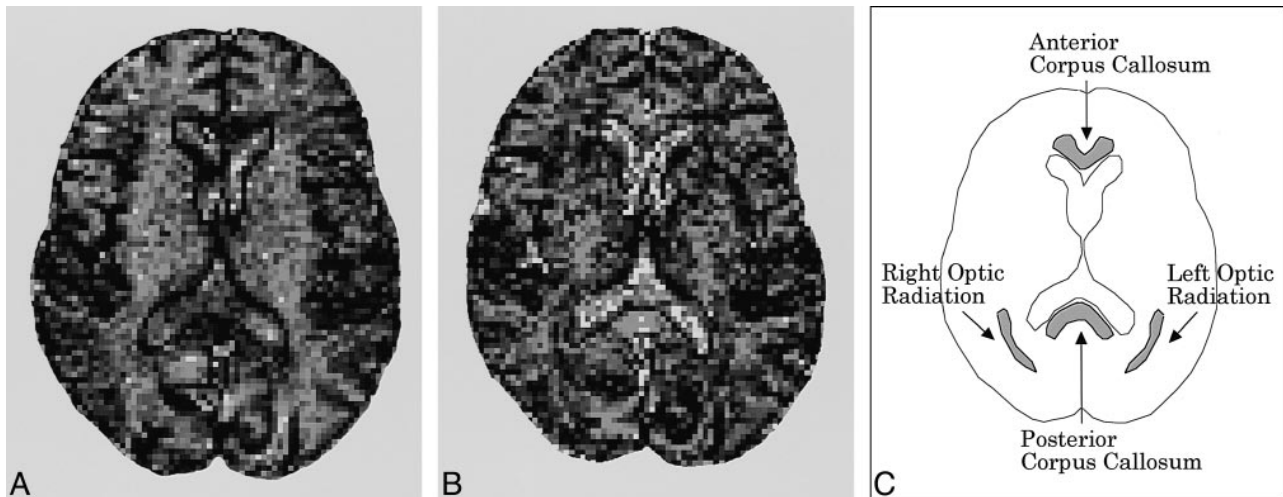
FIG 1.   A representative level of calculated ADC maps. ROIs, placed on the anterior and posterior corpus callosum and optic radiation, are 100 to 200 pixels each and the same in contour between the two maps.
A, ADC
B, ADC
C, A scheme for regional data extraction from these maps.

$$\text{ACV}(\%) = \frac{\text{(regional number of pixels in 80\% masking map)}}{\text{(regional number of pixels in the lower masking map)}} \times 100$$

The validity of this parameter was determined by testing whether these values eliminated partial volume effects using brain phantom (IB-10, Kyotokagaku-Hyohon, Kyoto, Japan) SPECT scans. SPECT scans were obtained using exactly the same protocol as in the human experiment described above, with ^{123}I-IMP concentration of gray matter and white matter of 7.8 MBq/530 mL and 2.2 MBq/300 mL (concentration rate = 2:1), respectively.

Using the original human SPECT scans, ROIs were specified in the superior and inferior frontal associative areas, the parietal associative area, and the temporal associative area, to exclude the primary sensorimotor area, mesial temporal lobe, or insula. These were then superimposed on the ACV maps (Fig 2). To determine whether these ACVs correlated with cognitive function, they were compared with the cognitive scores in the patient group. The ARs were then compared with these ACVs for all subjects to elucidate the relationship between the interhemispheric neuronal connectivity and cortical perfusion.

Statistical Analysis

Parametric variables were expressed as mean values ± SD. Regional differences between the ACVs within a group were compared using one-way analysis of variance corrected for multiple comparisons, and the intergroup differences between the ACVs as well as between the ARs were compared using unpaired two-tailed t-tests, with $P < .05$ representing statistical significance. Correlations between the ACV and MMSE scores within the patient group, and between the ACV and MR values of all subjects, were determined using linear regression analysis, also with $P < .05$ representing statistical significance.

Results

Determination of the Lower Masking Level for ACV Based on Human SPECT Scans

Figure 3 and Table 1 show the process of how the best lower masking level was determined. As shown in Table 1, the masked volume ratio at the 70% level was close to the ratio previously reported (49.5%) (17), and we selected that as the lower masking level.

Validation of ACV by Phantom SPECT Scans

Figure 4 shows phantom SPECT scans depicting eight different ROIs in various cortical regions. As shown in Table 2, the coefficient of variance of the ratio of the number of pixels above the 80% level to the number above the 70% level in these ROIs was much smaller than that of the number of pixels themselves, indicating that it reflects actual tracer accumulation regardless of the cortical regions.

Comparisons of Regional ACV between Groups

In terms of regional ACV differences, the lowest ACVs were observed in the frontal associative areas of the patient group; however, regional ACV differences were not significant in either the patient or volunteer groups. When regional ACVs were compared between the groups, there were significant decreases in the patients' ACVs in the superior frontal region, inferior frontal region, and temporal lobe ($P < .05$). These results are presented in Table 3. In the patient group, furthermore, individual ACVs in the superior and inferior frontal regions correlated well with the cognitive score (superior frontal: $r = .87$, $P < .05$; inferior frontal: $r = .73$, $P < .01$). These results are shown in Figure 5.

Comparisons of Regional Diffusional Anisotropy between Groups

In both groups, the AR was markedly larger in the corpus callosum than in the optic radiation, attributable to regional differences in diffusional anisotropy. Compared with the healthy group, how-

Fig 2. *A–D,* A representative series of binary SPECT scans showing masking levels of 60% (*A*), 65% (*B*), and 70% (*C*) of the maximal counts and the original SPECT scan (*D*). As the masking level increased, the number of masked pixels of relatively low counts also increased.
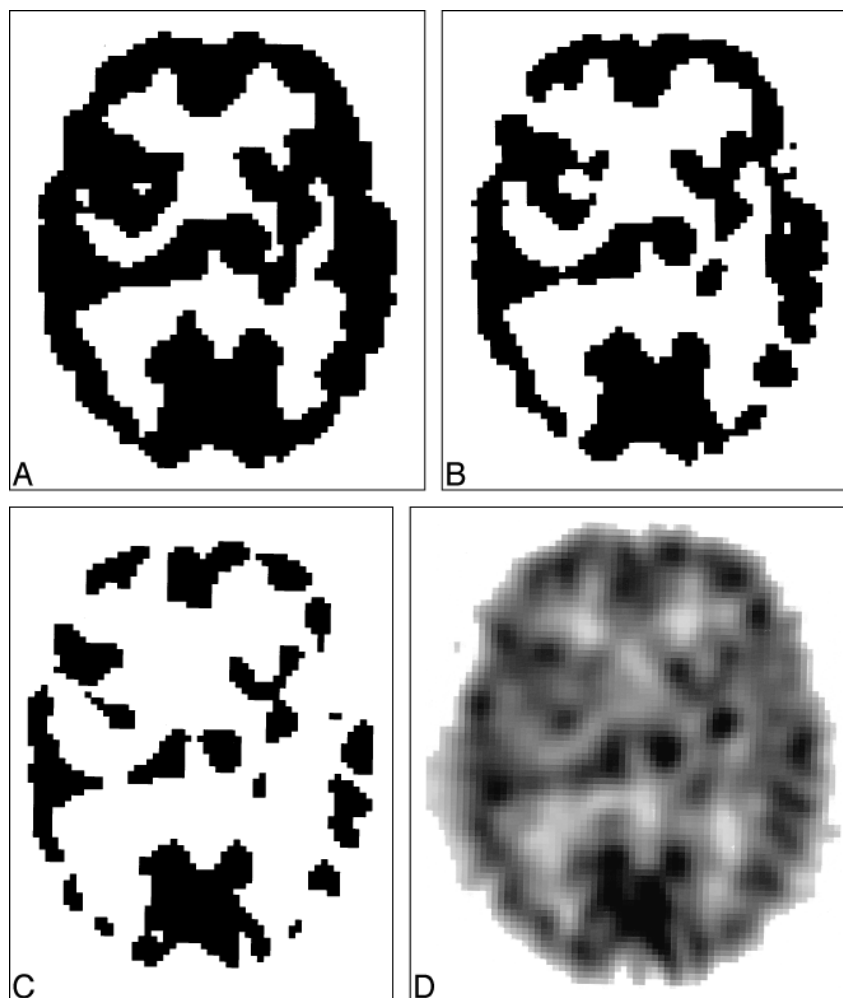
ever, there were significant decreases in the patients' ARs in the anterior and posterior parts of the corpus callosum ($P < .05$). Table 4 summarizes the regional ARs in both groups.

Relationship between Associative Cortical Activity and Neuronal Connectivity

Including the data of all participants, the AR in the anterior corpus callosum was strongly correlated with the frontal ACV (Fig 6) (superior frontal: $r = .86$, $P < .0001$; inferior frontal: $r = .79$, $P < .0005$). However, these correlations were insignificant within the group of patients with multiple lacunae, probably because of the limited number of patients in this study. No significant correlation was shown in the other combinations of the AR and the ACV.

Discussion

The main finding of this study suggests a possible relationship between diffusional anisotropy of the anterior corpus callosum and cortical activity of the frontal associative areas that are related to global cognitive function. Although the diffusional an-

isotropy parameter used did not provide adequate evidence of a loss in neuronal connectivity among the limited number of patients in our study, it did suggest that diffusion-weighted MR imaging might be useful not only for visualizing but also for evaluating functional relationships between cortical and subcortical structures.

The ACV parameter was used to compare SPECT data between patients and young healthy volunteers, comparisons that are often difficult to make because of changes in tracer accumulation as a function of structural atrophy. The reason for using the relative number of pixels of the two masking levels instead of a direct calculation of the number of pixels is that it is impossible to apply the same ROI size to the associative areas of individual brains. As shown in the phantom experiment, the ACV, determined as the ratio of the number of pixels above the 80% masking level to the number above the 70% level, reduced the variance of the cortical activity measurement because of partial volume effects. However, a potential error source in using this parameter is that it assumes that the tracer accumulation is relatively homogeneous, which is not the case for most diseased white matter. Another important error source is that
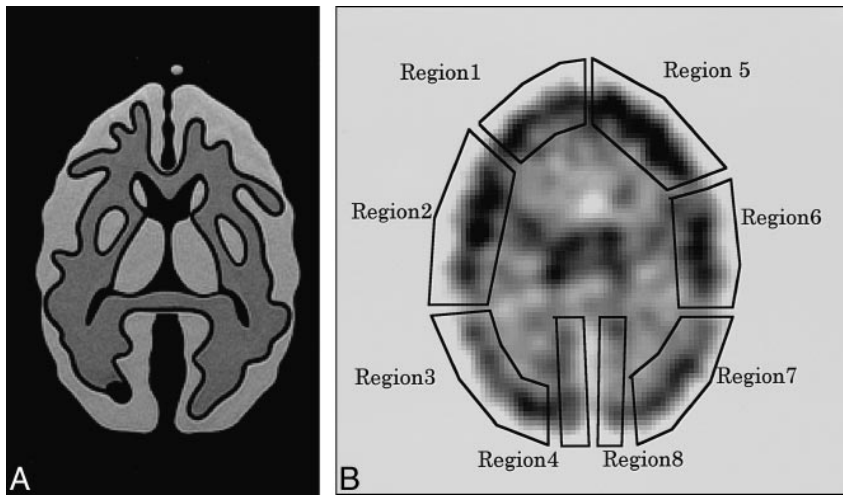
FIG 3. An explanation of how the ACV, determined as the ratio of the number of pixels above the 80% masking level to the number above the 70% level, is validated. In this setting, the ACVs derived from the eight cortical areas should be homogeneous, because the actual tracer accumulation in the cortical area is uniform regardless of the regions.

A, Phantom MR image.

B, Phantom ^{123}I-IMP SPECT scan.

Table 1: The *percentage* of masked pixels *to* total brain pixels among all participants using the three different masking levels

Masking level (%)	60	65	70
No. of pixels*	26.7 ± 5.9	22.3 ± 6.4	16.6 ± 5.8
Percentage of masked pixels†	14 ± 8	29 ± 11	48 ± 14

* Total = 31.0 ± 5.3.

† The number of masked pixels divided by the number of total pixels.

Table 2: Phantom simulation of the active cortical volume using 70% and 80% masking levels

	No. of Pixels		Active Cortical Volume (%)
	70% Level	80% Level	
Region 1	39	28	72
Region 2	66	44	67
Region 3	65	47	72
Region 4	76	54	71
Region 5	42	31	74
Region 6	44	32	73
Region 7	54	37	69
Region 8	63	44	70
Mean	56	40	71
SD	13	9	2
Coefficient of variance	0.2	0.2	0.03

it ignores the alteration in the gray matter/white matter ratio associated with aging. This especially affects the lower masking level, because a lower masking level that is too low (ie, one that is lower than the actual gray matter volume) induces underestimation of the ACV. On the other hand, a too-high lower masking level induces the inverse outcome. Recently, researchers in positron emission tomography have proposed an MR-based partial volume correction method, in which the actual radiotracer distributions are simulated by the convolution of each major structure based on MR imaging (18–20). Although this method requires a somewhat complicated computer simulation, we recommend further validation of this method using phantom data and implementation in actual brain images with a reference for comparison.

According to the previous study of diffusional anisotropy in patients with multiple lacunar infarction (11), in which variation of ADC_x and ADC_y of the anterior corpus callosum in patients with various cognitive levels was assessed, a decrease in the AR was attributable to an insignificant increase in the ADC_y as a function of disease severity (high
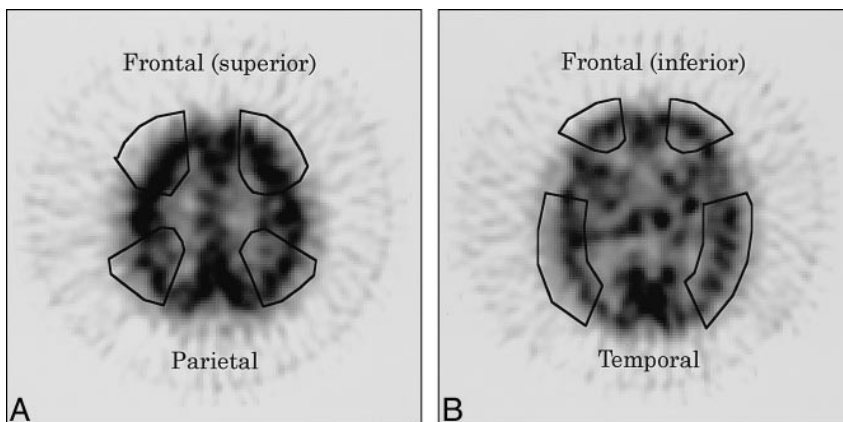

FIG 4. *A* and *B,* A representation of regional data extraction from one of the original SPECT scans. ROIs are specified at the superior frontal lobe and the parietal lobe (*A*), and the inferior frontal lobe and the temporal lobe (*B*), so as not to include the primary sensorimotor area, mesial temporal lobe, or insula. The ROIs are superimposed on ACV maps.

Table 3: Comparisons of the active cortical volume of the four associative areas between the healthy volunteer and patient groups

	Normal Volunteer	Patient
Frontal (*superior*)	42.8 ± 22.7	22.2 ± 12.8*
Frontal (*inferior*)	45.0 ± 14.3	26.3 ± 10.9*
Parietal	35.1 ± 12.2	26.5 ± 13.9†
Temporal	50.4 ± 11.4	31.3 ± 15.1*

* $P < .05$.

† Not significant.

Table 4: Comparisons of the regional anisotropic rate between the healthy volunteer and patient groups

	Normal Volunteer	Patient
Anterior corpus callosum	3.20 ± 1.26	1.79 ± 0.71*
Posterior corpus callosum	3.62 ± 0.92	2.09 ± 1.46*
Right optic radiation	0.56 ± 0.10	0.67 ± 0.20†
Left optic radiation	0.53 ± 0.11	0.49 ± 0.21†

* $P < .05$.

† Not significant.

cognitive level < low cognitive level), whereas the ADC_x change was insignificant. This result suggested to us that water diffusion in the *y*-axial direction, which is usually restricted by the myelin sheath, was increased because of a reduction in the number of nerve fibers, which has been observed in previous electron microscopy studies (3, 4). The current study further suggests that diffusional anisotropy of the anterior corpus callosum is related to the frontal associative function and thus possibly indicates the presence of functional networks between the frontal cortical and subcortical structures. However, it is unclear whether these findings are caused by increased extraaxonal space or increased CSF space (callosal atrophy) or both. These are relatively indistinguishable, because the diffusion co-

efficient of CSF is a few times larger than that of brain parenchyma (21), and contaminations of the pixels from the CSF space cannot be ignored, especially in the aging brain. Insignificant correlations between the AR and the frontal ACVs in patients with multiple lacunae might partly result from these contaminations. One solution for avoiding these contaminations would be to use the sequence of diffusion-weighted MR imaging with CSF-suppressed fluid-attenuated inversion recovery (21–23). Another explanation for these insignificant parameter correlations in the patient group might be a mathematically insufficient determination of diffusional anisotropy (24–27). The problem of characterizing diffusional anisotropy using the ratio of ADC values in two perpendicular di-
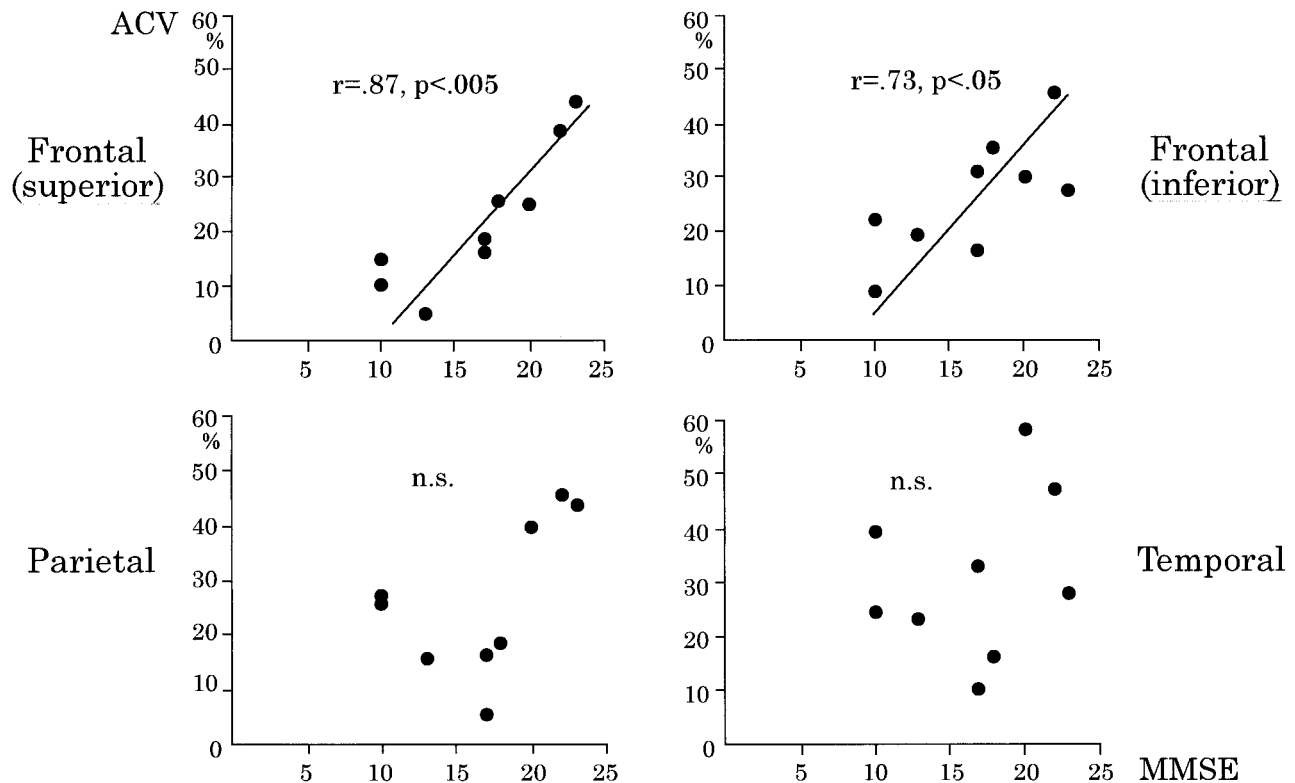

FIG 5.   Correlations between the regional ACV and the MMSE scores. Individual ACVs in the superior and inferior frontal regions were well correlated with the MMSE score (superior frontal: $r = .89$, $P < .05$; inferior frontal, $r = .71$, $P < .05$).
Left upper, superior frontal.
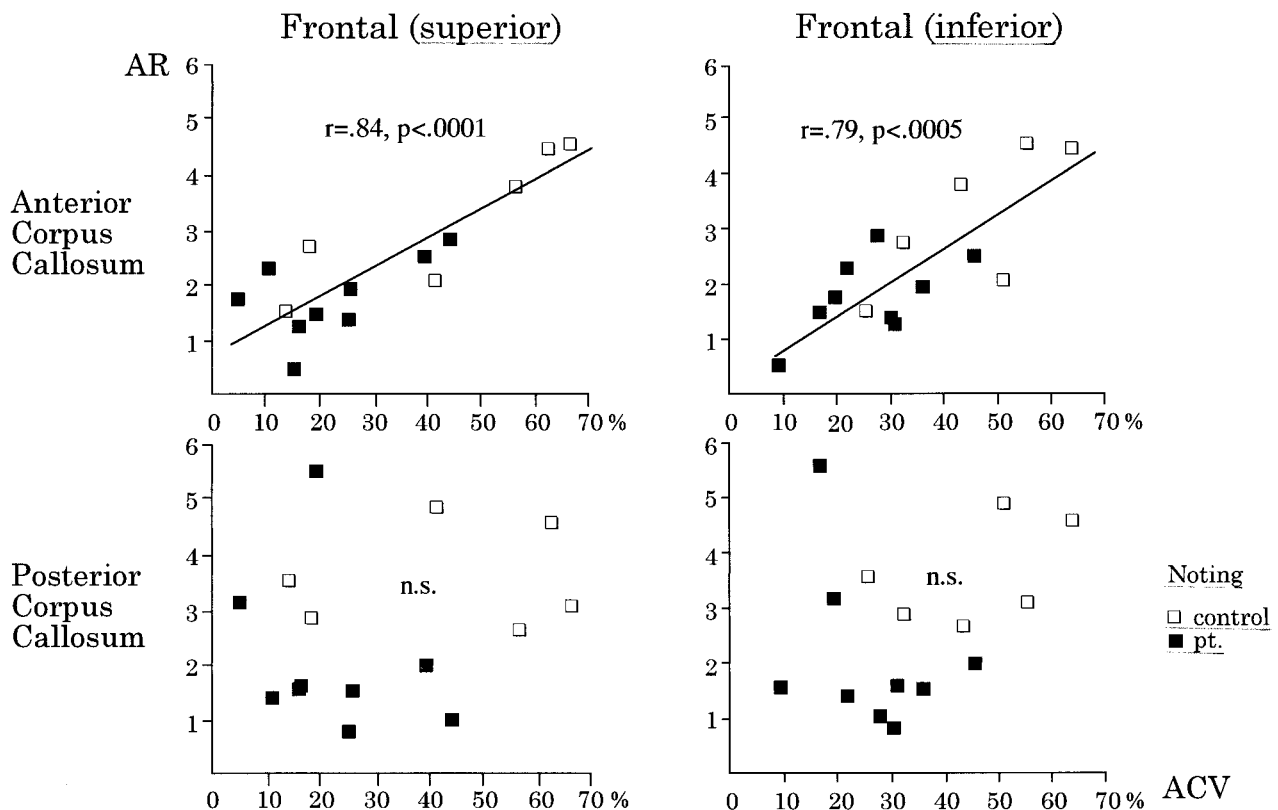*Right upper,* inferior frontal.
Left lower, parietal.
Right lower, temporal.

Fɪɢ 6. Correlations between the regional AR of the corpus callosum and the ACV of the frontal areas. The AR in the anterior corpus callosum is strongly correlated with the frontal ACVs (superior frontal: *r* = .86, *P* < .0001; inferior frontal: *r* = .79, *P* < .0005). However, there are insignificant trends toward correlation between the AR in the anterior corpus callosum and the frontal ACVs within the patient group.
Left upper, anterior corpus callosum versus superior frontal region.
Right upper, anterior corpus callosum versus inferior frontal region.
Left lower, posterior corpus callosum versus superior frontal region.
Right lower, posterior corpus callosum versus inferior frontal region.

rections has been discussed (24–27). It has already been reported that the magnitude of diffusional anisotropy of the corpus callosum derived from this index is up to three times lower than that estimated by the trace of the diffusion tensor (25). Therefore, calculation of the diffusion tensor of the anterior corpus callosum and other subcortical structures and assessment of its relation to the cortical associative function will be the next step of our study.

The findings revealed by diffusion-weighted MR imaging are based on structural alterations of nerve fibers. Thus, whether the quality of functional white matter connections can be implied from structural changes is an issue that has not been resolved. The important step would be to investigate the temporal relationship between the findings detected by diffusion-weighted MR imaging, the emergence of cortical perfusional changes, and the development of morphologic changes (atrophy). In other words, diffusion-weighted MR imaging may allow researchers to prove that functional neuroimaging data (1, 2) and postmortem neuropathologic data (3, 4) are related, and this knowledge may be clinically useful in terms of measuring disease progression. Further studies replicating our efforts in large groups of patients will offer important infor-

mation leading to greater understanding of how vascular dementia develops.

Conclusion

This study was conducted to evaluate loss of interhemispheric neuronal connectivity in a background disease of vascular dementia by measuring diffusional anisotropy of the corpus callosum and its relation to regional associative cortical activity. A positive correlation probably exists between diffusional anisotropy of the anterior corpus callosum and the frontal associative function; however, estimating the loss of neuronal connectivity in cases of multiple lacunar infarction in terms of the deterioration in diffusional anisotropy requires further study.

Acknowledgment

References
1. Yao H, Sadoshima S, Kuwabara Y, Ichiya Y, Fujishima M. **Cerebral blood flow and oxygen metabolism in patients with vas-**

cular dementia of the Binswanger type. *Stroke* 1990;21:1694–1699

2. Terayama Y, Meyer JS, Kawamura J, Weathers S, Mortel KF. **Patterns of cerebral hypoperfusion compared among demented and nondemented patients with stroke.** *Stroke* 1992;23:686–692

3. Yamanouchi H, Sugiura S, Tomonaga M. **Decrease in nerve fibers in cerebral white matter in progressive subcortical vascular encephalopathy of Binswanger type.** *J Neurol* 1989;236:382–387

4. Yamanouchi H, Sugiura S, Shimada H. **Loss of nerve fibres in the corpus callosum of progressive subcortical vascular encephalopathy.** *J Neurol* 1990;237:39–41

5. Le Bihan D, Breton E, Lallemand D, Grenier P, Cabanis E, Laval-Jeantet M. **MR imaging of intravoxel incoherent motions: application to diffusion and perfusion in neurologic disorders.** *Radiology* 1986;161:401–407

6. Le Bihan D, Breton E, Lallemand D, Aubin ML, Vibnaud J, Laval-Jeantet M. **Separation of diffusion and perfusion in intravoxel incoherent motion MR imaging.** *Radiology* 1988;168:497–505

7. Turner R, Le Bihan D, Maier J, Vavrek R, Hedges LK, Pekar J. **Echo-planar imaging of intravoxel incoherent motion.** *Radiology* 1990;177:407–414

8. Moseley ME, Cohen Y, Kucharczyk J, et al. **Diffusion-weighted MR imaging of anisotropic water diffusion in cat central nervous system.** *Radiology* 1990;176:439–446

9. Chenevert TL, Brunberg JA, Pipe JG. **Anisotropic diffusion within human white matter: demonstration with NMR techniques in vivo.** *Radiology* 1990;177:401–405

10. Le Bihan D, Turner R, Douek P. **Is water diffusion restricted in human brain white matter? An echo-planar NMR imaging study.** *Neuroreport* 1993;4:887–890

11. Ishihara M, Hayashi H, Amano Y, et al. **Assessment of diffusional anisotropy of the corpus callosum in patients with multiple lacunar infarcts: relationship between the apparent diffusion coefficient ratio and global cognitive impairment.** *Jpn J Magn Reson Med* 1998;18:204–211

12. De Reuck J, Crevits L, De Coster W, Sieben G, vander Eecken H. **Pathogenesis of Binswanger chronic progressive subcortical encephalopathy.** *Neurology* 1980;30:920–928

13. Mazziotta JC, Phelps ME, Plummer D, Kuhl DE. **Quantitation in positron emission computed tomography, 5: physical-anatomical effects.** *J Comput Assist Tomogr* 1981;5:734–743

14. Videen TO, Perlmutter JS, Mintun MA, Raichle ME. **Regional correction of positron emission tomography data for the ef-**fects of cerebral atrophy. *J Cereb Blood Flow Metab* 1988;8:662–670

15. Douek P, Turner R, Pekar J, Patronas N, Le Bihan D. **MR color mapping of myelin fiber orientation.** *J Comput Assist Tomogr* 1991;15:923–929

16. Sakuma H, Nomura Y, Takeda K, et al. **Adult and neonatal human brain: Diffusion anisotropy and myelination with diffusion-weighted MR imaging.** *Radiology* 1991;180:229–233

17. Harris GJ, Barta PE, Peng LW, et al. **MR volume segmentation of gray matter and white matter using manual thresholding: dependence on image brightness.** *AJNR Am J Neuroradiol* 1994;15:225–230

18. Meltzer CC, Leal JP, Mayberg HS, Wagner Jr HN, Frost JJ. **Correction of PET data for partial volume effects in human cerebral cortex by MR imaging.** *J Comput Assist Tomogr* 1990;14:561–570

19. Mueller-Gartner HW, Links JM, Prince JL, et al. **Measurement of radiotracer concentration in brain gray matter using positron emission tomography: MRI-based correction for partial volume effects.** *J Cereb Blood Flow Metab* 1992;12:571–583

20. Meltzer CC, Zubieta JK, Links JM, Brakeman P, Stumpf MJ, Frost JJ. **MR-based correction of brain PET measurements for heterogeneous gray matter radioactivity distribution.** *J Cereb Blood Flow Metab* 1996;16:650–658

21. Falconar JC, Narayana PA. **Cerebral fluid-suppressed high-resolution diffusion imaging of human brain.** *Magn Reson Med* 1997;37:119–123

22. Kwong K.K, McKinstry RC, Chien D, Crawley AP, Pearlman JD, Rosen BR. **CSF-suppressed quantitative single-shot diffusion imaging.** *Magn Reson Med* 1991;21:157–163

23. Ishihara M, Hayashi H, Amano Y, et al. **Assessment of deterioration in diffusional anisotropy of commissural association fibers using diffusion-weighted echo planar imaging with FLAIR in patients with multiple lacunar infarctions.** Presented at the annual meeting of the International Society of Magnetic Resonance in Medicine, Sydney, Australia, April 1998

24. Basser PJ, Mattiello J, Le Bihan D. **MR diffusion tensor spectroscopy and imaging.** *Biophys J* 1994;66:259–267

25. Pierpaoli C, Jezzard P, Basser PJ, Barnett A, Di Chiro G. **Diffusion tensor MR imaging of the human brain.** *Radiology* 1996;201:637–648

26. Basser PJ, Pierpaoli C. **Microstructural and physiological features of tissues elucidated by quantitative-diffusion-tensor MRI.** *J Magn Reson B* 1996;111:209–219

27. Pierpaoli C, Basser PJ. **Toward a quantitative assessment of diffusion anisotropy.** *Magn Reson Med* 1996;36:893–906